PCCP

ROYAL SOCIETY OF CHEMISTRY

PAPER

View Article Online
View Journal | View Issue

Cite this: *Phys. Chem. Chem. Phys.*, 2020, **22**, 4501

Isomer-specific cryogenic ion vibrational spectroscopy of the D_2 tagged $Cs^+(HNO_3)(H_2O)_{n=0-2}$ complexes: ion-driven enhancement of the acidic H-bond to water†

Sayoni Mitra, [a] Chinh H. Duong, [a] Laura M. McCaslin, [bc] R. Benny Gerber *[bc] and Mark A. Johnson *[a]

Received 12th December 2019,
Accepted 5th February 2020

DOI: 10.1039/c9cp06689f

rsc.li/pccp

We report how the binary $HNO_3(H_2O)$ interaction is modified upon complexation with a nearby Cs^+ ion. Isomer-selective IR photodissociation spectra of the D_2-tagged, ternary $Cs^+(HNO_3)H_2O$ cation confirms that two structural isomers are generated in the cryogenic ion source. In one of these, both HNO_3 and H_2O are directly coordinated to the ion, while in the other, the water molecule is attached to the OH group of the acid, which in turn binds to Cs^+ with its $-NO_2$ group. The acidic OH stretching fundamental in the latter isomer displays a $\sim$300 cm^{-1} red-shift relative to that in the neutral H-bonded van der Waals complex, $HNO_3(H_2O)$. This behavior is analyzed with the aid of electronic structure calculations and discussed in the context of the increased effective acidity of HNO_3 in the presence of the cation.

I. Introduction

Nitric acid (HNO_3) plays an important role in the chemistry of the atmosphere,[1,2] ranging from ozone depletion in polar regions[3,4] to the regeneration of pollutants in the troposphere through reactions mediated by sea spray aerosol (SSA) particles.[5–8] Accurately describing the behavior of HNO_3 in such complex environments is challenging because it involves the molecular level treatment of a strong acid at the air–water interface in the presence of aqueous inorganic ions (alkali and alkaline earth metals, halides, carboxylates, *etc.*).[9–23] In this report, we adopt a bottom up approach to establish key paradigms driving the HNO_3 response to the local environment, and in particular explore how the fundamental interaction between HNO_3 and one water molecule is modified by the presence of a bare Cs^+ cation as well as by the $Cs^+(H_2O)$ monohydrate. This information is obtained by analyzing the vibrational spectra of the isolated $Cs^+(HNO_3)(H_2O)_{n=0-2}$ cluster ions, obtained using infrared, cryogenic photofragmentation mass spectrometry. Our specific focus is to determine the distortions in the intrinsic HNO_3/H_2O binary interaction induced by attachment to a Cs^+ cation.

The high resolution microwave spectrum of the neutral (van der Waals) $HNO_3(H_2O)$ complex[24] has been analyzed to yield the structure indicated in Fig. 1b. In this arrangement, the acid OH group is attached to a lone pair of electrons on the water molecule in the entrance channel of the endoergic ($\sim$8.7 kcal mol^{-1}) acid–base reaction (refer to Table S1, ESI†). Electronic structure calculations predict that attachment of a Cs^+ ion to the neutral complex occurs in the two isomeric forms denoted B1 and B2 in Fig. 1d and e, respectively. In the B1 structure, the binary HNO_3/H_2O interaction is enhanced, while in the other (isomer B2), the two neutral constituents are broken apart and attach directly onto the ion in its first solvation shell. In this report, we capture both of these forms in the laboratory and report the resulting spectral responses of both the water molecule and the nitric acid in each form. It is of particular interest to assess the degree to which the acidity of the OH group on the acid is enhanced by electrostatic stabilization of the incipient $-(NO_3)^{\delta-}$ group by a proximal cation in structure B1, as well as the effects of H_2O and its binding location.

II. Experimental and computational methods

Vibrational spectra of the size-selected $Cs^+(HNO_3)(H_2O)_{n=0-2}$ complexes were obtained in an action mode with IR photodissociation (IRPD) of weakly bound D_2 adducts. This was carried out using the Yale cryogenic photofragmentation mass spectrometer.[25] Briefly, this method involves cooling the ion of interest in a cryogenic ion trap held at $\sim$30 K to enable

[a] *Sterling Chemistry Laboratory, Yale University, New Haven, CT, USA. E-mail: chinh.duong@yale.edu, mark.johnson@yale.edu*
[b] *Department of Chemistry, University of California Irvine, Irvine, CA, USA. E-mail: bgerber@uci.edu*
[c] *Institute of Chemistry and the Fritz-Haber Center for Molecular Dynamics, The Hebrew University, Jerusalem, Israel*

† Electronic supplementary information (ESI) available. See DOI: 10.1039/c9cp06689f

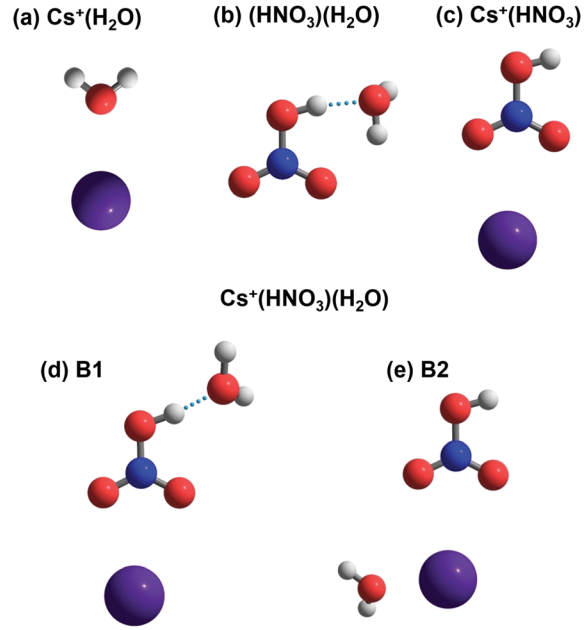

Fig. 1 Calculated structures for the binary complexes (a) $Cs^+(H_2O)$, (b) $HNO_3(H_2O)$ and (c) $Cs^+(HNO_3)$, along with two isomers of the ternary $Cs^+(HNO_3)(H_2O)$ cluster ion, denoted as B1 and B2, in (d) and (e).

condensation of weakly bound D_2 molecules. Predissociation spectroscopy using the D_2 "tag" allows efficient mass separation between parent ion and the photofragment, and D_2 has been shown to be a good compromise with respect to ease of execution (compared to He), while introducing minimal perturbation to the ion of interest.[26–28] The linear action spectrum is then acquired by single photon-induced photoevaporation of the D_2 "mass tag" (Fig. S1, ESI†). Minimum energy structures were calculated using "Gaussian 09,[42] with" the B3LYP[29] density functional and aug-cc-pVDZ[30] basis for all atoms but Cs, for which the LANL2DZ[31] basis and corresponding pseudopotential were used. All reported energies are zero point energy corrected at their stationary point with this level of theory. All bare and calculated structures of interest are presented in Fig. S2 (ESI†). Single point energies were calculated at the CCSD(T)[32,33] level of theory with the same basis and pseudopotential described above. The harmonic frequencies are scaled by a factor of 0.9956 for frequencies above 1850 cm^{-1} and 0.9719 for those below. All other calculations were performed in Q-Chem with the exception of the CCSD(T) calculations, which were performed in CFOUR.[34] Further experimental details are provided in Section S1 (ESI†).

III. Results and discussion

III.A. Survey spectra of the D_2 tagged $Cs^+(HNO_3)(H_2O)_{n=0-2}$ ions in the OH stretching region

The top trace (Fig. 2a) displays the spectrum of the binary $Cs^+(HNO_3)$ complex, which exhibits features arising from the acidic OH group (denoted ν^a) near 3500 cm^{-1}, as well as from the D_2 tag (ν^{D_2}, near 3000 cm^{-1}). Although the IR fundamental

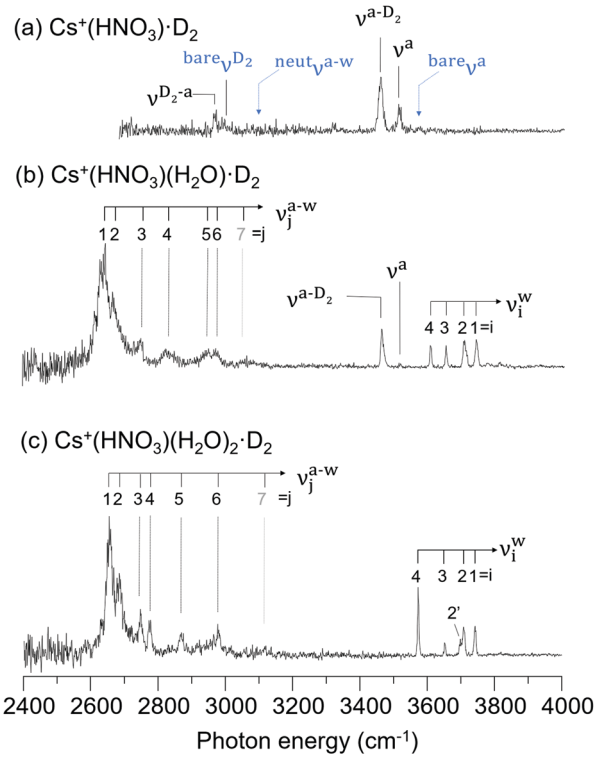

Fig. 2 The vibrational predissociation spectra of $Cs^+(HNO_3)(H_2O)_n{\cdot}D_2$ are presented in traces (a)–(c) for n = 0, 1 and 2, respectively. The ν^a and $\nu^{a\text{-}D2}$ refer to the free acid O–H stretch and the O–H stretch bound to D_2 respectively, for both the $Cs^+(HNO_3){\cdot}D_2$ and $Cs^+(HNO_3)(H_2O){\cdot}D_2$ complexes. The ν_i^w denote the water O–H vibrational bands, where i = 1–4, and similarly, acid O–H stretches are represented by $\nu_j^{a\text{-}w}$, for $Cs^+(HNO_3)(H_2O){\cdot}D_2$ and $Cs^+(HNO_3)(H_2O)_2{\cdot}D_2$, respectively, where '$j$' = 1–7 represents the vibrational progressions. The blue bands ${}^{bare}\nu^{D2}$, ν_1^w and ${}^{bare}\nu^a$ are described in Table S2 (ESI†).

of the isolated D_2 molecule is nominally forbidden by electric dipole selection rules, in the presence of an ion, the D_2 vibrational coordinate is associated with a weak degree of intracluster charge transfer. The telltale signature of this effect is that the transition dipole vector direction lies perpendicular to the D–D internuclear axis, which is predicted to be the case in our calculated spectra for these clusters.[26] The OH stretch appears as an asymmetric doublet with a separation of ~56 cm^{-1}, with the dominant band occurring ~40 cm^{-1} below the OH fundamental in isolated HNO_3 (${}^{bare}\nu^a$, blue arrow in Fig. 2a). Such multiplet structure typically signals the formation of different isomers that result from the location of the D_2 tag, an issue addressed in detail below. The evolution of the spectra upon addition of the first two water molecules is presented in Fig. 2b and c. The hydrates are both dominated by a very strong band ($\nu_1^{a\text{-}w}$) near 2650 cm^{-1} which appears with a progression of weaker bands ($\nu_j^{a\text{-}w}$) above the main feature. In addition, new sharp features appear on the high energy side of the OH stretching region in the vicinity expected for the fundamentals associated with a water molecule.

The strongest band in the monohydrate is readily assigned to the acidic OH stretch, for which the large (~900 cm^{-1}

relative to the isolated acid) red-shift and intensity enhancement is expected for (scaled) harmonic spectrum (Fig. S10b, ESI†) of the sandwich structure B1, in which the water molecule accepts a strong H-bond from the acid OH group. This is the motif that occurs in the binary $HNO_3(H_2O)$ complex, for example, where the OH stretching fundamental of the acid ($^{neut}\nu^{a\text{-}w}$, Table S2, ESI†), occurs about 450 cm^{-1} below that of the free acid, as indicated by the arrow in Fig. 2a. This indicates that addition of the Cs^+ ion to the $HNO_3(H_2O)$ complex (Fig. 2b) leads to an increase in the red-shift of the acidic OH group ($\nu_1^{a\text{-}w}$) by almost a factor of two. In addition to the red-shifted acid OH stretch, however, the $Cs^+(HNO_3)(H_2O)\cdot D_2$ spectrum (Fig. 2b) also displays a sharp feature in essentially the same location as the D_2-tagged acid OH stretch ($\nu^{a\text{-}D_2}$) in the binary $Cs^+(HNO_3)$ complex. The ternary cluster also displays four sharp bands in the OH stretching region typically associated with water molecules bound by accepting an H-bond. A different four-band pattern is observed upon addition of the second water molecule (Fig. 2c), while the strong $\nu_1^{a\text{-}w}$ feature near 2650 cm^{-1} is retained. Finally, the acid OH stretch ($\nu^{a\text{-}D_2}$) disappears in the spectrum of the dihydrate, indicating that this OH group is always complexed to one of the water molecules. This behavior is easily rationalized in a scenario where, in the monohydrate, two hydration positions are available, which are both occupied upon addition of the second water molecule.

III.B. Isomer-specific spectroscopy

To establish the possible contributions of one or more isomers to the observed spectra in Fig. 2, we turn to isomer-selective IR photodissociation (IRPD) spectroscopy. This requires excitation with two tunable IR lasers and three stages of mass-selection, and hence is denoted an IR^2MS^3 class of IR photodissociation action spectroscopy.[35–37] Briefly, one laser (the probe) is fixed on a particular transition and its photofragment is monitored continuously to detect the population of the isomer responsible for this feature. A second powerful IR laser (the pump) is then scanned upstream from the probe, and any transition driven by the pump laser removes the population of the isomer associated with it. If this photodissociated isomer corresponds to the one interrogated by at the probe transition, the probe fragment yield is depleted, and the spectrum associated with the probed isomer is revealed as series of dips in the probe signal as the pump laser is scanned through the spectrum.

III.B.1 $Cs^+(HNO_3)$. Application of the IR^2MS^3 method to the $Cs^+(HNO_3)\cdot D_2$ spectrum is presented in Fig. 3. Probing at the two bands as indicated in Fig. 3a yields the two dip traces in Fig. 3b and c, confirming that the spectrum is heterogeneous. Relative to the isolated HNO_3 $^{bare}\nu^a$, the more red-shifted $\nu^{a\text{-}D_2}$ band (by 94 cm^{-1}, Tables S2 and S3, ESI†) is consistent with its assignment to an isomer in which D_2 binds to the OH group; this arrangement is calculated to be the lowest energy form ($A1\cdot D_2$) with the structure displayed in the inset in Fig. 3b. A second isomer ($A2\cdot D_2$) was recovered with the calculated structure indicated in the inset in Fig. 3c, which features D_2 tag attachment to the Cs^+ ion. As such, the acid OH group is free, accounting for the higher energy OH stretch (ν^a in Fig. 3c).

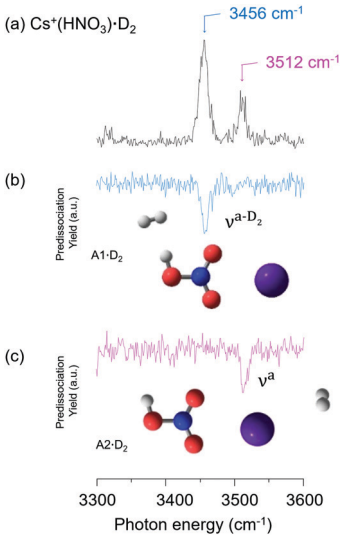

Fig. 3 Isomer-selective IR^2MS^3 spectra of the $Cs^+(HNO_3)\cdot D_2$ cluster probed at (b) 3456 cm^{-1} and (c) 3512 cm^{-1}, corresponding to the two bands in the region of the acid OH stretch, reproduced from Fig. 2a in panel (a). The isomers ($A1\cdot D_2$ and $A2\cdot D_2$), consistent with the locations of the two OH bands, are presented as insets in (b) and (c), respectively, thus establishing that the lower energy band is due to the OH bound to the D_2 molecule.

The fact that the latter band is weakest supports the theoretical prediction that the $A2\cdot D_2$ isomer lies 0.56 kcal mol^{-1} above $A1\cdot D_2$. Structural details for the two calculated structures are presented in Fig. S2 (panels (a) and (e)) (ESI†).

Returning to the acidic OH activity in the spectrum of the D_2-tagged, binary Cs^+HNO_3 complex, the assignment of the weaker feature to the free acid stretch, ν^a, indicates that bidentate HNO_3 complexation with Cs^+ (as shown in Fig. 1c) yields a $\sim$38 cm^{-1} red-shift relative to the band in the free acid ($^{bare}\nu^a$). This is anticipated at the harmonic level for the structure in Fig. 1c, which predicts the NOH bond angle to close by 3° and the OH bond to elongate by 0.01 Å upon complexation with the cation.

III.B.2 $Cs^+(HNO_3)(H_2O)$. Fig. 4 presents the IR^2MS^3 spectra obtained for the (D_2-tagged) $Cs^+(HNO_3)(H_2O)$ ternary cluster. The single laser IRPD spectrum is reproduced in Fig. 4a, while the fragment signal arising from setting the probe laser at two different transitions (ν_1^w, blue at 3741 cm^{-1} and $\nu^{a\text{-}D_2}$, pink at 3464 cm^{-1}) are displayed in Fig. 4c and e, respectively. The two probe transitions yield dramatically different dip patterns, thus establishing that the single laser spectrum (Fig. 4a) is a superposition of contributions from two isomers (denoted B1 and B2), with the bands from each color-coded in Fig. 4a. The B1 form can be immediately identified by the strongly red-shifted $\nu_1^{a\text{-}w}$ band in Fig. 4c, which also accounts for two of the OH bands associated with the attached water molecule (ν_1^w and ν_3^w). The dip spectrum of the other isomer (Fig. 4e) recovers the D_2-tagged, free acid feature ($\nu^{a\text{-}D_2}$) along with two other bands arising from the water OH stretches (ν_2^w and ν_4^w). These spectra are consistent with the predicted behavior of the calculated (scaled) harmonic spectra (bars in Fig. 4b and d) for the minimum

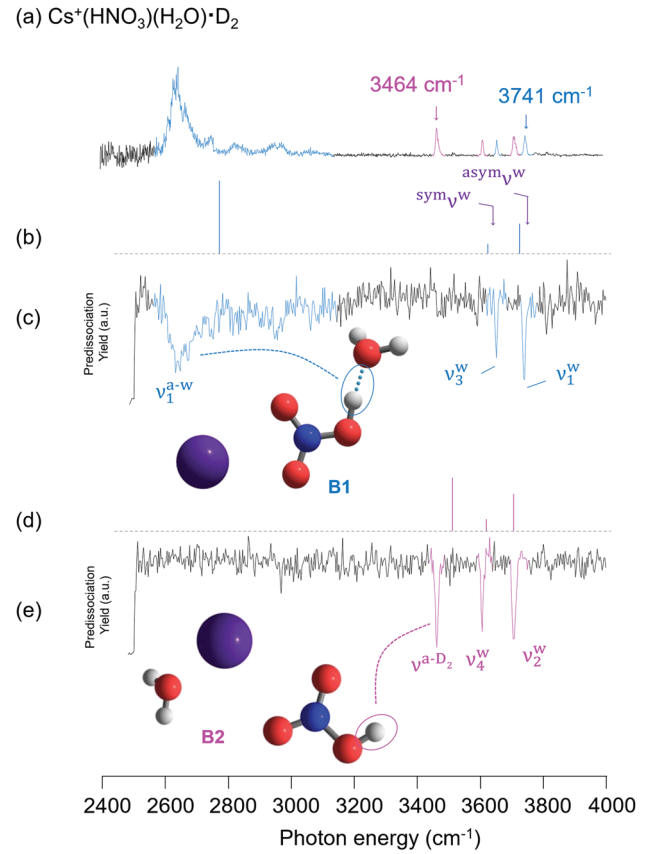

Fig. 4 Isomer-specific spectra of the $Cs^+(HNO_3)(H_2O)\cdot D_2$ cluster using two-color, IR–IR hole-burning. Predissociation spectrum of $Cs^+(HNO_3)(H_2O)\cdot D_2$ is shown in (a), with the depletion traces (c) and (e) obtained by probing at the positions indicated by arrows in (a). The calculated harmonic spectra of the isomers B1 and B2 are (b) and (d), as described in the Experimental and computational methods section. In (c), bands ν_1^w and ν_3^w correspond to acid-bound H_2O O–H symmetric and asymmetric stretches, while $\nu_1^{a\text{-}w}$ is the water-bound acid O–H stretch. In (e), bands ν_2^w and ν_4^w correspond to Cs^+ ion bound H_2O O–H symmetric and asymmetric stretches, while $\nu^{a\text{-}D2}$ is the D_2-bound acid O–H stretch.

energy structures displayed in the insets of Fig. 4 and presented in more detail in Fig. S2 (ESI†) in the panels (b), (c), (f) and (g).

The OH stretch of the acidic OH group bound to the water molecule in the isomer B1 spectrum ($\nu_1^{a\text{-}w}$ in Fig. 4c) is interesting in that this represents a $\sim$450 cm^{-1} red-shift compared to ($^{neut}\nu^{a\text{-}w}$) displayed by the neutral binary complex (Fig. S3, ESI†). This shift thus provides a direct measurement of the enhancement in the effective HNO_3 acidity by the presence of the positively charged Cs^+ attached to the $-NO_2$ group. We discuss this effect further in Section III.C.

The appearance of a weaker progression of peaks above the dominant $\nu_1^{a\text{-}w}$ band ($\nu_i^{a\text{-}w}$ in Fig. 2b) is often encountered in the spectra of strong H-bonds.[38,39] This occurs when the OH frequency is strongly modulated by displacements along the soft modes associated with frustrated rotation and translation of the tethered water molecule. The ($\sim$100 cm^{-1}) spacing of the $\nu_i^{a\text{-}w}$ bands (see values in Table S4, ESI†) is consistent with the calculated frequencies of various soft modes at the harmonic level.

In both isomers of the monohydrate (B1 and B2), the bands associated with the water molecule in the OH stretching region are unambiguously assigned to fundamentals of the symmetric (ν_3^w,ν_4^w) and antisymmetric (ν_1^w,ν_2^w) stretching normal modes of the two OH groups in each isomer, respectively. In the isomer B1 structure, the H_2O molecule hydrogen bonds with the acid O–H group, whereas in B2, the water molecule resides in the first solvation shell around the Cs^+ ion along with HNO_3, leaving the acid OH group free. The red-shifts in the O–H stretches of the H_2O molecule bound to the ion in isomer B2 place these bands considerably below those of both bare water (broken arrows in Fig. 4b) and those of the more distant H_2O molecule in isomer B1. This red-shift is typical for O–H oscillators in the strong positive electric field close to the Cs^+ ion, and largely reflects the fact that the magnitude of the dipole moment along the OH bond increases with bond length.[40] A complete picture of the H_2O O–H oscillator shifts is seen in Fig. S4 (ESI†). We remark that the two isomers are formed by water attachment to either the acid OH group or to the Cs^+ ion, which are the same two locations adopted by the more weakly bound D_2 molecule.

The fact that the two $Cs^+(HNO_3)(H_2O)$ isomers in the monohydrate are prepared with about equal abundance indicates that there must be a substantial barrier to interconversion. Interestingly, our calculations indicate that B1, in which the water molecule resides in the second solvation shell, is lowest in energy, with the B2 form predicted to lie $\sim$3.1 kcal mol^{-1} above it. Note that the relative abundance of the isomers is not one that is expected for an equilibrium distribution at low temperature, indicating the populations are "locked in" at relatively high energy during the cooling process. The calculated structure of the transition state is presented in Fig. S5 (ESI†), with energy 3.5 kcal mol^{-1} above that of B2.

III.B.3 $Cs^+(HNO_3)(H_2O)_2$. Double resonance spectra were also recorded for the dihydrate (Fig. S6, ESI†), which established that this cluster only occurs in one isomeric form. This behavior is readily explained by the structure depicted in Fig. S2, panels (d) and (h) (ESI†), where the two water molecules occupy both positions established as preferred docking sites by the two isomers from the monohydrate. Interestingly, however, the spectrum is not a simple superposition of those associated with the two isomers. In particular, the lowest member of the quartet (ν_4^w) is clearly both red-shifted (by $\sim$30 cm^{-1}) and enhanced relative to the pattern displayed in Fig. 2a. The implications of this discrepancy will be discussed in the context of the calculated structures in Section III.C. All band assignments for the mid-IR region are presented in Tables S2–S5 (ESI†).

III.C. Structural deformation of the acid upon ion complexation and microhydration

To address how the heavy atoms of the acid respond to complexation, we turn to the low frequency region of the spectrum with the results for the three ions displayed in Fig. 5. The D_2 tagged $Cs^+(HNO_3)$ system (Fig. 5a) is dominated by bands readily assigned to the HO–N stretch (ν_{HO-N}^a) near 950 cm^{-1} and those at $\sim$1350 and 1660 cm^{-1} are derived from the symmetric $^{sym}\nu_{NO_2}^a$ and antisymmetric $^{asym}\nu_{NO_2}^a$ collective modes of the $-NO_2$ group,

anchored to the ion in a bidentate manner. The latter two fundamentals are split apart by about 350 cm^{-1}, which is about 50 cm^{-1} smaller than those in the free acid.[41] The breadth and multiplet structures of these features is expected in light of the similar contributions from the two isomers (A1 and A2) identified above arising from the location of the D_2 tag. The only exception is the OH bending mode, ν^{a}_{bend}, which is calculated to yield a substantial ($\sim$50 cm^{-1}) blueshift in the A1·D_2 isomer in which D_2 attaches to the acidic OH group and accounts for the band $\nu^{a\text{-}D_2}_{bend}$ near 1300 cm^{-1}. The predicted contributions from the two isomers are indicated in red and blue highlights in the calculated spectra presented by the vertical bars in Fig. 5a, and provide compelling assignments of all features in the observed spectrum (inverted trace in Fig. 5a).

These spectral changes in the HNO_3 fundamentals upon ion complexation are summarized in Fig. 6c, and point to a scenario where partial negative charge is accumulated on the $-NO_2$ moiety. This leads to a $\sim$3° contraction of the ONO bond angle as well as a 0.03 Å shortening of the N–OH bond length, which brings the core structure of the O–NO_2 scaffold closer to that of the NO_3^- anion (Fig. 6e). Nominal charges on the atoms and the detailed structural deformation of the acid molecule upon complexation with the cation are included in Fig. S7 and S8 (ESI†) to further explore this interplay between the electronic and structural contributions to the electric polarizability of the acid in response to the strong electric field of the ion.

With the behavior of the binary Cs^+HNO_3 complex in mind, we consider the additional deformation in the acid constituent upon hydration to yield the B1 isomer of the ternary complex. The contributions from both isomers are readily assigned from the predicted (scaled) harmonic spectra, and are highlighted by the blue (B1) and red (B2) inverted bars in Fig. 5b. The intramolecular bends of the water molecule are clearly split apart in the two spectra with the water closest to the ion (B2) yielding the higher energy member of the doublet near 1650 cm^{-1}. We note that the scaling factor which was derived from the Cs^+HNO_3 behavior substantially overestimates the

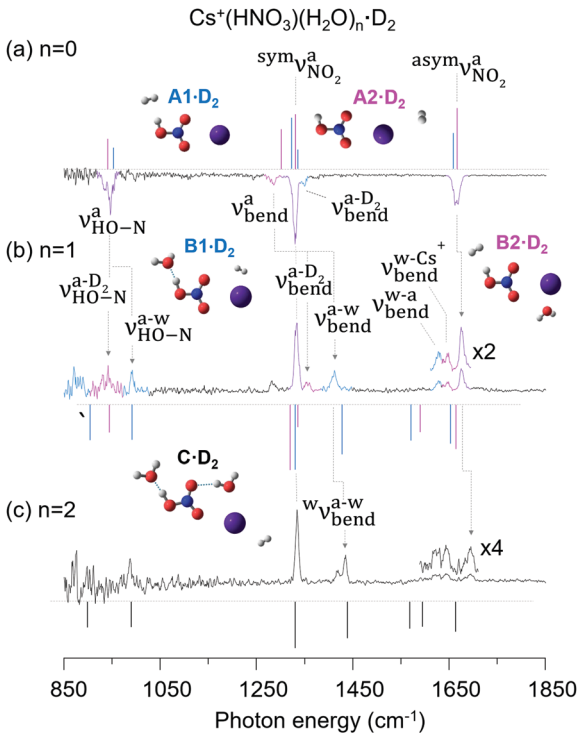

Fig. 5 The vibrational predissociation spectra of $Cs^+(HNO_3)(H_2O)_n·D_2$ in the fingerprint region are presented in traces (a)–(c) for n = 0, 1 and 2, respectively, along with the stick spectra for the isomer (or isomers) associated with each, as elucidated before. The ν^{a}_{HO-N} band is the HO–N stretch and ν^{a}_{bend} is the acid NO–H bend of the HNO_3 molecule in the A2·D_2 isomer of the $Cs^+(HNO_3)·D_2$ complex, while $\nu^{a\text{-}D_2}_{bend}$ band is the acid NO–H bend of the HNO_3 molecule in A1·D_2 isomer. Bands $\nu^{a\text{-}D_2}_{HO-N}$ and $\nu^{a\text{-}D_2}_{bend}$ are the HO–N stretch and acid NO–H bend of the HNO_3 molecule in B2·D_2 isomer of $Cs^+(HNO_3)(H_2O)·D_2$ complex, while bands $\nu^{a\text{-}w}_{HO-N}$ and $\nu^{a\text{-}w}_{bend}$ are the HO–N stretch and acid NO–H bend of the HNO_3 molecule in B1·D_2 isomer. Calculated stick spectra are obtained as described in the Experimental and computational methods section, and all bands assignments are presented in Tables S6–S9 (ESI†).

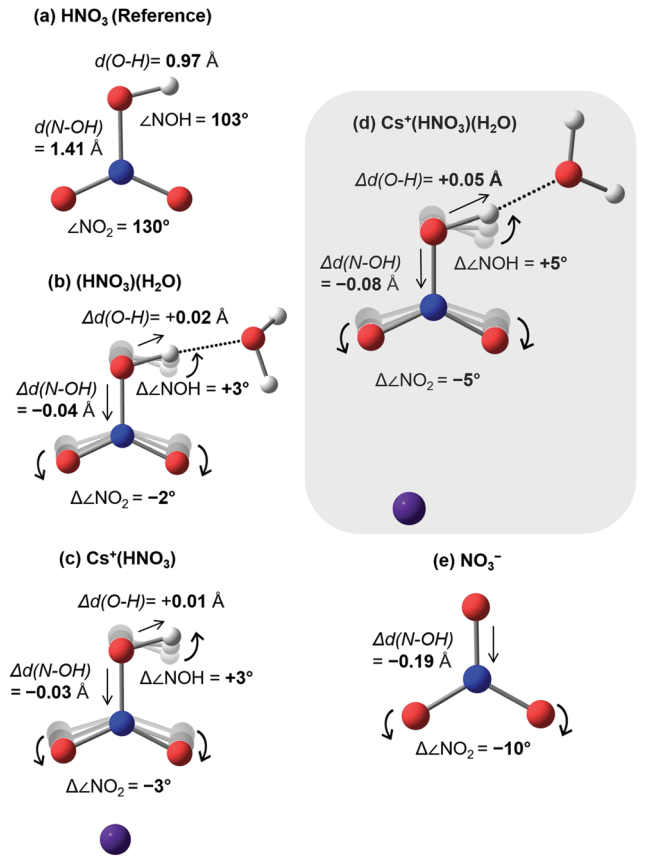

Fig. 6 The distortion in the geometry (exaggerated for illustration purposes) of (a) an isolated HNO_3 molecule is studied under the influence of H_2O in (b), Cs^+ ion in (c), and the combined effect of Cs^+ ion and H_2O molecule in (d), while (e) presents the structure of the isolated NO_3^- anion. All shifts are denoted relative to the HNO_3 molecule. Note that the $-NO_2$ angle (denoted $\angle NO_2$) and the NO–H bond distance (d(NO–H)) decrease such that they become more similar to those in nitrate in structure (d). The net distortion of the acid is a combination of the independent effects from the ion and the water molecule, revealing the cooperative mechanics underlying ion-assisted proton transfer.

red-shift experienced by the water molecule in either site. The most significant changes upon hydration involve the substantial ($\sim$40 cm^{-1}) blue shift of the N–OH stretch near 960 cm^{-1} as well as the 120 cm^{-1} blue shift of the NOH bend $\nu_{\mathrm{bend}}^{\mathrm{a\text{-}w}}$ around 1410 cm^{-1} (see Fig. 5b). Interestingly, these changes upon monohydration are essentially amplified variations of the spectral shifts that occurred between the two D_2 isomers of the Cs^+HNO_3 binary complex, A1 and A2, as well as those displayed upon complexation of the bare HNO_3 molecule to Cs^+. This effect is highlighted in Fig. 6d, which schematically indicates the collective distortion of the HNO_3 scaffold when sandwiched between the ion and the water molecule. This suggests that the system is exploring the entrance channel of the intracluster frustrated proton transfer reaction,[38] where the proton transfer configuration is substantially enhanced when the cation can stabilize electronic configurations featuring excess charge accumulation onto the NO_3^- moiety.

Finally, we note that the structure of the dihydrate (Fig. 5c) is predicted to occur with insertion of a water molecule in the first hydration shell of the Cs^+ ion between one of the –NO–Cs^+ contacts by donating a hydrogen bond to one of the oxygen atoms of the acid NO group. As such, a productive direction for future study of these ion-driven acid–base mechanics will be to follow how the acid solvation mechanics evolve with smaller alkali ions as well as stronger bases, such as alcohols and ethers.

IV. Summary

We have isolated and structurally characterized two isomeric forms of the $Cs^+(HNO_3)(H_2O)$ complex by analyzing their vibrational spectra with electronic structure calculations. The spectra were obtained by application of isomer-specific cryogenic ion infrared photodissociation spectroscopy. One of the structures corresponds to complexation of the water molecule and nitric acid directly to the ion, while in the other the acid is sandwiched between the ion and the water molecule. These minima in the potential surface are calculated to be separated by a barrier of about 1224 cm^{-1}. The acidic OH stretching fundamental of the latter isomer exhibits a very large ($\sim$450 cm^{-1}) red shift relative to that of the neutral $HNO_3(H_2O)$ binary complex, demonstrating the substantial enhancement of the acidity upon attachment of the Cs^+ ion to the –NO_2 group. Structural deformations of the HNO_3 framework are encoded in patterns of the low frequency vibrational modes, and reveal a picture in which both the ion and the water molecule induce collective heavy particle displacements expected for the nuclear contribution to the electrical polarizability. Hydration of the ternary system leads to a single isomer in which the sandwich structure of the ternary complex is preserved while the second water molecule adds to the first hydration shell of the Cs^+ ion, inducing a structural change in the –NO_2 attachment motif from a bidendate arrangement toward preferential attachment to one of the oxygen atoms.

Conflicts of interest

There are no conflicts of interest to declare.

Acknowledgements

The authors would like to thank NSF Center for Aerosol Impacts on Chemistry of the Environment (CAICE), CHE-1801971, for support of this work. Any opinions, findings, and conclusions or recommendations expressed in this material are those of the author(s) and do not necessarily reflect the views of the National Science Foundation (NSF). L. M. M. would like to thank the Zuckerman STEM Leadership Program for support. C. H. D. thanks the National Science Foundation Graduate Research Fellowship for funding under Grant No. DGE-1122492.

References

1 S. Solomon, *Nature*, 1990, **347**, 347–354.
2 J. R. Huber, *ChemPhysChem*, 2004, **5**, 1663–1669.
3 C. Voigt, J. Schreiner, A. Kohlmann, P. Zink, K. Mauersberger, N. Larsen, T. Deshler, C. Kroger, J. Rosen, A. Adriani, F. Cairo, G. Di Donfrancesco, M. Viterbini, J. Ovarlez, H. Ovarlez, C. David and A. Dornbrack, *Science*, 2000, **290**, 1756–1758.
4 S. Solomon, *Rev. Geophys.*, 1999, **37**, 275–316.
5 M. Mochida and B. J. Finlayson-Pitts, *J. Phys. Chem. A*, 2000, **104**, 9705–9711.
6 N. A. Saliba, H. Yang and B. J. Finlayson-Pitts, *J. Phys. Chem. A*, 2001, **105**, 10339–10346.
7 S. Ghosal and J. C. Hemminger, *J. Phys. Chem. B*, 2004, **108**, 14102–14108.
8 P. Beichert and B. J. FinlaysonPitts, *J. Phys. Chem.*, 1996, **100**, 15218–15228.
9 P. Jungwirth and D. J. Tobias, *Chem. Rev.*, 2006, **106**, 1259–1281.
10 H. Mishra, S. Enami, R. J. Nielsen, M. R. Hoffmann, W. A. Goddard and A. J. Colussi, *Proc. Natl. Acad. Sci. U. S. A.*, 2012, **109**, 10228–10232.
11 H. Mishra, S. Enami, R. J. Nielsen, L. A. Stewart, M. R. Hoffmann, W. A. Goddard and A. J. Colussi, *Proc. Natl. Acad. Sci. U. S. A.*, 2012, **109**, 18679–18683.
12 J. K. Denton, P. J. Kelleher, M. A. Johnson, M. D. Baer, S. M. Kathmann, C. J. Mundy, B. A. Wellen Rudd, H. C. Allen, T. Choi and K. D. Jordan, *Proc. Natl. Acad. Sci. U. S. A.*, 2019, **116**, 14874–14880.
13 H. Mishra, R. J. Nielsen, S. Enami, M. R. Hoffmann, A. J. Colussi and W. A. Goddard III, *Int. J. Quantum Chem.*, 2013, **113**, 413–417.
14 E. S. Shamay, V. Buch, M. Parrinello and G. L. Richmond, *J. Am. Chem. Soc.*, 2007, **129**, 12910–12911.
15 M. H. Kuo, A. David, N. Kamelamela, M. White and M. J. Shultz, *J. Phys. Chem. C*, 2007, **111**, 8827–8831.
16 T. Lewis, B. Winter, A. C. Stern, M. D. Baer, C. J. Mundy, D. J. Tobias and J. C. Hemminger, *J. Phys. Chem. C*, 2011, **115**, 21183–21190.
17 J. J. Gilligan and A. W. Castleman, *J. Phys. Chem. A*, 2001, **105**, 5601–5605.
18 R. Bianco, S. Z. Wang and J. T. Hynes, *J. Phys. Chem. A*, 2008, **112**, 9467–9476.
19 M. F. Bush, J. T. O'Brien, J. S. Prell, R. J. Saykally and E. R. Williams, *J. Am. Chem. Soc.*, 2007, **129**, 1612–1622.

20 S. Z. Wang, R. Bianco and J. T. Hynes, *Comput. Theor. Chem.*, 2011, **965**, 340–345.
21 S. Z. Wang, R. Bianco and J. T. Hynes, *J. Phys. Chem. A*, 2009, **113**, 1295–1307.
22 N. Heine, E. G. Kratz, R. Bergmann, D. Schofield, K. R. Asmis, K. D. Jordan and A. B. McCoy, *J. Phys. Chem. A*, 2014, **118**, 8188–8197.
23 N. Heine, T. I. Yacovitch, F. Schubert, C. Brieger, D. M. Neumark and K. R. Asmis, *J. Phys. Chem. A*, 2014, **118**, 7613–7622.
24 M. Canagaratna, J. A. Phillips, M. E. Ott and K. R. Leopold, *J. Phys. Chem. A*, 1998, **102**, 1489–1497.
25 A. B. Wolk, C. M. Leavitt, E. Garand and M. A. Johnson, *Acc. Chem. Res.*, 2014, **47**, 202–210.
26 M. Z. Kamrath, E. Garand, P. A. Jordan, C. M. Leavitt, A. B. Wolk, M. J. Van Stipdonk, S. J. Miller and M. A. Johnson, *J. Am. Chem. Soc.*, 2011, **133**, 6440–6448.
27 J. W. DePalma, P. J. Kelleher, L. C. Tavares and M. A. Johnson, *J. Phys. Chem. Lett.*, 2017, **8**, 484–488.
28 M. Z. Kamrath, R. A. Relph, T. L. Guasco, C. M. Leavitt and M. A. Johnson, *Int. J. Mass Spectrom.*, 2011, **300**, 91–98.
29 A. D. Becke, *J. Chem. Phys.*, 1993, **98**, 1372–1377.
30 R. A. Kendall, T. H. Dunning, Jr. and R. J. Harrison, *J. Chem. Phys.*, 1992, **96**, 6796–6806.
31 P. J. Hay and W. R. Wadt, *J. Chem. Phys.*, 1985, **82**, 299–310.
32 K. Raghavachari, G. W. Trucks, J. A. Pople and M. Head-Gordon, *Chem. Phys. Lett.*, 1989, **157**, 479–483.
33 R. J. Bartlett, J. D. Watts, S. A. Kucharski and J. Noga, *Chem. Phys. Lett.*, 1990, **165**, 513–522.
34 J. G. J. F. Stanton, L. Cheng, M. E. Harding, D. A. Matthews, P. G. Szalay, w. c. from, R. J. B. A. A. Auer, U. Benedikt, C. Berger, D. E. Bernholdt, Y. J. Bomble, F. E. O. Christiansen, R. Faber, M. Heckert, O. Heun, M. Hilgenberg, T.-C. J. C. Huber, D. Jonsson, J. Jusélius, T. Kirsch, K. Klein, F. L. W. J. Lauderdale, T. Metzroth, L. A. Mück, D. P. O'Neill, E. P. D. R. Price, C. Puzzarini, K. Ruud, F. Schiffmann, W. Schwalbach, S. S. C. Simmons, A. Tajti, J. Vázquez, F. Wang, J. D. Watts, a. t. i. packages, MOLECULE (J. Almlöf and P.R. Taylor), PROPS (P.R. Taylor), H. J. A. J. ABACUS (T. Helgaker, P. Jørgensen, and J. Olsen), and a. E. r. b. A. V. M. a. C. v. Wüllen.
35 N. Yang, C. H. Duong, P. J. Kelleher, M. A. Johnson and A. B. McCoy, *Chem. Phys. Lett.*, 2017, **690**, 159–171.
36 C. H. Duong, O. Gorlova, N. Yang, P. J. Kelleher, M. A. Johnson, A. B. McCoy, Q. Yu and J. M. Bowman, *J. Phys. Chem. Lett.*, 2017, **8**, 3782–3789.
37 C. H. Duong, N. Yang, P. J. Kelleher, M. A. Johnson, R. J. DiRisio, A. B. McCoy, Q. Yu, J. M. Bowman, B. V. Henderson and K. D. Jordan, *J. Phys. Chem. A*, 2018, **122**, 9275–9284.
38 S. M. Craig, F. S. Menges, C. H. Duong, J. K. Denton, L. R. Madison, A. B. McCoy and M. A. Johnson, *Proc. Natl. Acad. Sci. U. S. A.*, 2017, **114**, E4706–E4713.
39 C. J. Johnson, L. C. Dzugan, A. B. Wolk, C. M. Leavitt, J. A. Fournier, A. B. McCoy and M. A. Johnson, *J. Phys. Chem. A*, 2014, **118**, 7590–7597.
40 G. G. Kebede, P. D. Mitev, W. J. Briels and K. Hermansson, *Phys. Chem. Chem. Phys.*, 2018, **20**, 12678–12687.
41 G. E. Mcgraw, D. L. Bernitt and I. C. Hisatsune, *J. Chem. Phys.*, 1965, **42**, 237–244.
42 M. J. Frisch, G. W. Trucks, H. B. Schlegel, G. E. Scuseria, M. A. Robb, J. R. Cheeseman, G. Scalmani, V. Barone, G. A. Petersson, H. Nakatsuji, X. Li, M. Caricato, A. Marenich, J. Bloino, B. G. Janesko, R. Gomperts, B. Mennucci, H. P. Hratchian, J. V. Ortiz, A. F. Izmaylov, J. L. Sonnenberg, D. Williams-Young, F. Ding, F. Lipparini, F. Egidi, J. Goings, B. Peng, A. Petrone, T. Henderson, D. Ranasinghe, V. G. Zakrzewski, J. Gao, N. Rega, G. Zheng, W. Liang, M. Hada, M. Ehara, K. Toyota, R. Fukuda, J. Hasegawa, M. Ishida, T. Nakajima, Y. Honda, O. Kitao, H. Nakai, T. Vreven, K. Throssell, J. A. Montgomery, Jr., J. E. Peralta, F. Ogliaro, M. Bearpark, J. J. Heyd, E. Brothers, K. N. Kudin, V. N. Staroverov, T. Keith, R. Kobayashi, J. Normand, K. Raghavachari, A. Rendell, J. C. Burant, S. S. Iyengar, J. Tomasi, M. Cossi, J. M. Millam, M. Klene, C. Adamo, R. Cammi, J. W. Ochterski, R. L. Martin, K. Morokuma, O. Farkas, J. B. Foresman and D. J. Fox, *Gaussian 09, Revision A.02*, Gaussian, Inc., Wallingford CT, 2016.